



저작자표시-비영리-변경금지 2.0 대한민국

이용자는 아래의 조건을 따르는 경우에 한하여 자유롭게

- 이 저작물을 복제, 배포, 전송, 전시, 공연 및 방송할 수 있습니다.

다음과 같은 조건을 따라야 합니다:



저작자표시. 귀하는 원저작자를 표시하여야 합니다.



비영리. 귀하는 이 저작물을 영리 목적으로 이용할 수 없습니다.



변경금지. 귀하는 이 저작물을 개작, 변형 또는 가공할 수 없습니다.

- 귀하는, 이 저작물의 재이용이나 배포의 경우, 이 저작물에 적용된 이용허락조건을 명확하게 나타내어야 합니다.
- 저작권자로부터 별도의 허가를 받으면 이러한 조건들은 적용되지 않습니다.

저작권법에 따른 이용자의 권리는 위의 내용에 의하여 영향을 받지 않습니다.

이것은 [이용허락규약\(Legal Code\)](#)을 이해하기 쉽게 요약한 것입니다.

[Disclaimer](#)

**Three-dimensionally printed biphasic calcium phosphate
blocks with different pore diameters for regeneration in
rabbit calvarial defects**

Young-Wook Seo

Department of Dentistry

The Graduate School, Yonsei University

**Three-dimensionally printed biphasic calcium phosphate
blocks with different pore diameters for regeneration in
rabbit calvarial defects**

Directed by Professor Seong-Ho Choi

The Doctoral Dissertation
submitted to the Department of Dentistry
and the Graduate School of Yonsei University
in partial fulfillment of the requirements for the degree of
Ph.D. in Dental Science

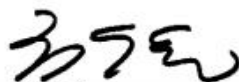
Young-Wook Seo

December 2022

This certifies that the Doctoral Dissertation
of Young-Wook Seo is approved.



Thesis Supervisor: Seong-Ho Choi



Ui-Won Jung



Jung-Seok Lee



Jae-Kook Cha



Jeong-Won Paik

The Graduate School
Yonsei University
December 2022

감사의 글

먼저, 본 연구가 학위 논문으로 완성이 되기까지 여러 면에서 부족한 저를 사랑과 격려의 마음으로 지도해주시고 이끌어주신 최성호교수님께 진심으로 감사드립니다. 아울러, 저의 치주과 수련 및 대학원 재학 중의 은사님들이신 조규성, 김창성, 정의원, 이중석, 차재국, 백정원, 송영우, 박진영 교수님께 깊이 감사를 드립니다.

3년이라는 시간 동안 함께 고생하며 열심히 공부한 의국원들과 실험을 진행하는 데에 많은 도움을 준 연구원 선생님들에게도 감사의 마음을 전합니다.

항상 변함없이 아낌없는 사랑으로 제게 항상 힘을 주는 사랑하는 아내 윤진에게 감사의 마음과 사랑의 뜻을 전합니다. 그리고 넘치는 사랑과 격려의 마음으로 변함없는 응원을 해주신 양가 부모님과 양가 형제, 자매들에게도 사랑과 감사의 마음을 전합니다.

2022년 12월

저자 서영욱

TABLE OF CONTENTS

List of figures	iii
List of tables	iv
Abstract (English)	v
I. INTRODUCTION	1
II. MATERIALS AND METHODS	4
1. Materials	4
2. Animals	4
3. Study design	5
4. Sample size determination	5
5. Surgical procedure	6
6. Analysis	6
III. RESULTS	10
1. Clinical observations	10
2. Micro-CT volumetric analysis	10
3. Histomorphometric analysis	11
4. Histological observations	11

IV. DISCUSSION	14
V. CONCLUSION	18
REFERENCE	19
TABLES	22
FIGURES	24
Abstract (Korean)	31

List of figures

- Figure 1.** Structural design 3D- printed biphasic calcium phosphate(BCP) block bone substitutes.
- Figure 2.** BCP block fabrication process by Digital Light Processing (DLP).
- Figure 3.** Microstructure surface images of 3D-printed BCP block using scanning electron microscopy (SEM, 3.0kV)
- Figure 4.** Study design and reconstructed images at 2- and 8-weeks.
- Figure 5.** Comparison of A new bone volume(NBV) by micro-CT analysis and new bone area(NBA) by histomorphometric analysis at 2- and 8-weeks.
- Figure 6.** Micro-CT views at 2- and 8-weeks of healing period.
- Figure 7.** Histomorphometric views at 2- and 8-weeks of healing period.

List of tables

Table 1. The results from micro-CT analysis.

Table 2. The results from histomorphometric analysis.

Abstract

**Three-dimensionally printed biphasic calcium phosphate
blocks with different pore diameters for regeneration in
rabbit calvarial defects**

Young-Wook Seo, D.D.S., M.S.

*Department of Dentistry
The Graduate School, Yonsei University*

(Directed by Professor Seong-Ho Choi, D.D.S., M.S.D., PhD.)

Purpose: The aim of this study was to compare three-dimensionally printed biphasic calcium phosphate (BCP) block bone substitutes with different pore diameters (0.8-, 1.0-, and 1.2- mm) for use in the regeneration of rabbit calvarial defects.

Methods: This study used 3D printed BCP blocks with various pore diameters. The BCP consisted of HA and β -TCP at a 60:40 ratio, and had pore diameters of 0.8, 1.0, and 1.2 mm. The 3D-printed block bone substitutes were prepared using a digital light processing 3D printer. Four circular defects were formed on the calvaria of ten rabbits. Each defect was randomly allocated to one of the following study groups: (i) control group,

(ii) 0.8-mm group, (iii) 1.0-mm group, and (iv) 1.2-mm group. All specimens were postoperatively harvested at 2 and 8 weeks, and radiographic and histomorphometric analyses were performed on the samples.

Results: Histologically, the BCP blocks remained unresorbed up to 8 weeks, and new bone formation occurred within the porous structures of the blocks. After the short healing period of 2 weeks, histomorphometric analysis indicated that new bone formation was significantly greater in the BCP groups compared with the control ($p<0.05$). However, there were no significant differences between the groups with different pore diameters ($p>0.05$). At 8 weeks, only the 1.0-mm group (3.42 ± 0.48 mm², mean \pm standard deviation) presented a significantly larger area of new bone compared with the control (2.26 ± 0.59 mm²) ($p<0.05$). Among the BCP groups, the 1.0- and 1.2-mm groups exhibited significantly larger areas of new bone compared with the 0.8-mm group (3.42 ± 0.48 and 3.04 ± 0.66 vs 1.60 ± 0.70 mm², respectively)

Conclusion: Within the limitations of this study, the BCP block bone substitutes can be applied to bone defects for successful bone regeneration. In the 1.0mm pore diameter BCP block, regeneration was promoted by fusion between new bones, showing the most bone regeneration results among the experimental groups. Future studies should investigate more-challenging defect configurations prior to considering clinical applications

Keywords: Animals; Bone regeneration; Pore diameter; Hydroxyapatite; Beta tri-calcium phosphate

Three-dimensionally printed biphasic calcium phosphate blocks with different pore diameters for regeneration in rabbit calvarial defects

Young-Wook Seo, D.D.S, M.S.

*Department of Dentistry
The Graduate School, Yonsei University*

(Directed by Professor Seong-Ho Choi, D.D.S., M.S.D., Ph.D.)

I. INTRODUCTION

Alveolar ridge augmentation is frequently performed on deficient alveolar ridges to facilitate dental implant placement (Barone, Aldini et al. 2008, Chavda and Levin 2018, Lee, Cha et al. 2018). Severe resorption of the bony ridge may occur due to aging or periodontal and periapical pathologies. In this situation, a block bone graft is suggested since the block bone provides structural stability to the augmented site. Autogenous block bone has been considered the gold standard due to its combined osteogenic, osteoinductive, and osteoconductive properties. However, there are also disadvantages including additional

surgical procedures for block harvesting, the surgery is technically difficult, and donor-site morbidity might occur(Roccuzzo, Ramieri et al. 2007).

Nowadays, computer-aided design and computer aided manufacturing (CAD/CAM) or three-dimensional (3D) printing technology are frequently applied to produce medical devices. In dentistry, these processes are routinely used for the fabrication of dental prosthesis and surgical templates. The benefits of 3D printing such devices include reduction of time and cost of manufacture. Furthermore, the convenience of fabrication can significantly improve clinical efficiency. Recently, the application of 3D printing has expanded to the production of biomaterials. By doing so, block-type bone graft materials can be customized to fit into individual defects, and characteristics of the biomaterial such as the chemical composition and porosity, can be adjusted.

Biphasic calcium phosphate (BCP) is the most frequently used synthetic bone substitutes, which comprises a combination of hydroxyapatite (HA) and beta-tricalcium phosphate (β -TCP)(Kato, Lemler et al. 2014). Calcium phosphate is the natural chemical constituent of the living bone, and so BCP exhibits excellent biocompatibility. The HA component provides the osteoconductive scaffold for cell migration, vascularization, and new bone formation(De Oliveira, De Aguiar et al. 2003, Hwang, Park et al. 2012, Ramesh, Moratti et al. 2018), while β -TCP is more biodegradable and is the source of calcium and phosphate ions for bone formation(Kato, Lemler et al. 2014).

The presence of interconnected pores in the BCP block is vital since they allow cell infiltration and vascularization(Hing 2005, Lim, Chian et al. 2010, Roosa, Kemppainen et al. 2010, Cheng, Wahafu et al. 2016). The diameter of the pores can influence the rate of bone formation and material resorption. Previous studies have found that larger pores result in more-rapid bone formation(Gauthier, Bouler et al. 1998, Chang, Lee et al. 2000, Lim, Hong et al. 2020), which is due to greater space for initial bone formation and the larger surface area of the material exposed to osteoclast resorption(Kato, Lemler et al. 2014). However, it can be hypothesized that if the pore diameter exceeds a certain threshold, then

the osteoconductivity of BCP will be outweighed by the ingrowth of fibrous tissues into the BCP block combined with biomaterial degradation. Numerous studies have attempted to determine the optimal pore diameter for bone formation, but the results have been inconclusive(Gauthier, Bouler et al. 1998, Chang, Lee et al. 2000, Diao, OuYang et al. 2018).

In this study, BCP-block-type substitutes with pore diameters of 0.8, 1.0, and 1.2 mm were fabricated using 3D printing. Our hypothesis was that synthetic BCP block bone substitute with the largest 1.2-mm pores will facilitate the greatest amount of bone formation when placed in a bone defect. The aim of this study was to compare BCP blocks with different pore diameters for the regeneration of rabbit calvarial defects..

II. MATERIALS AND METHODS

1. Materials

This study used 3D printed BCP blocks with various pore diameters. The BCP consisted of HA and β -TCP at a 60:40 ratio, and had pore diameters of 0.8, 1.0, and 1.2 mm. The 3D-printed block bone substitutes were prepared using a digital light processing 3D printer (Cubicon Lux, Cubicon®, Sungnam, Korea) which has a resolution of 20-100 μm and can print layers that are 20–100 μm thick. This 3D printer guarantees an accuracy of 20 μm in the z- axis and 65 μm in the xy- axis. Before production of the specimen, a preliminary sample of 5x5x5 cube was printed, sintered and inspected. The horizontal plane of the print was checked at inspection process. All specimens were designed by using computer software program (Materialise 3-Matic, Proto3000®, Ontario, Canada) and manufactured by stacking the BCP layer with the same diamond crystal lattice sphere structure with a thickness of 20 to 100 μm (Fig 1). The manufacturing process was as follows (Fig. 2): The bone substitute designs (diameter of 8 mm \times depth of 2 mm) were first converted into a stereolithography file that was used by the 3D printer to form the bone substitutes in a layer-by-layer manner. Ceramic slurries containing HA / β -TCP powder, acrylic monomer, dispersant, and photocatalyst were prepared. The UV light emitted from the projector of the printer was then reflected by the mirror through the lens on to the ceramic slurry while it was being printed by the build plate. Thereafter, the residual monomers were completely removed using in-furnace heat treatment at 1250°C for 10 hours (Carbolite, Ubstadt-Weiher, Germany) (Fig.3).

2. Animals

Ten New Zealand White rabbits (12 weeks old and weighing 2.8–3.2 kg) were used in the experiments. Animals were housed in separate cages under standard laboratory conditions and diet. The animals underwent an acclimatization period of 1 week prior to the experiments. The housing protocol was based on the guidelines of the Association for Assessment and Accreditation of Laboratory Animal Care International. All of the procedures for animal selection, care, and preparation for anesthesia and surgical procedures followed the protocol approved by the Institutional Animal Care and Use Committee of Yonsei Medical Center, Seoul, Korea.

3. Study design

Four circular bone defects with diameters of 8 mm were formed on the calvaria of the 10 rabbits. Each defect was randomly allocated to one of the following experimental groups (Fig. 4 A&B):

- (i) control group, empty;
- (ii) 0.8-mm group, BCP block with 0.8-mm pore diameter;
- (iii) 1.0-mm group, BCP block with 1.0-mm pore diameter;
- (iv) 1.2-mm group, BCP block with 1.2-mm pore diameter;

All subjects in this study were euthanized at 2 and 8 weeks after the bone graft procedure, and microcomputed tomography (micro-CT) analysis, histomorphometric analysis, and histological observations were performed on the experimental specimens.

4. Sample size determination

The sample sized was calculated based on a previous study(Pae, Kang et al. 2019) using a dedicated program (G*Power 3.1.9.4, Germany). For each group, it was estimated that five rabbits would be required under the significance level of 5% and the power of 80%.

5. Surgical procedure

A surgical procedure was performed based on those in previously reported study(Pae, Kang et al. 2019). General anesthesia was performed using isoflurane (2.0–2.5%) inhalation and alfaxan (5 mg/kg) and medetomidine (0.25 mg/kg) intravenous injections. Orotracheal intubation was performed using 6-mm tubes without ballooning to secure the airway. The surgical site was disinfected using povidone-iodine, and local anesthesia was performed using 2% lidocaine with a 1:80,000 epinephrine injection. After making an incision along the cranium midline, a full-thickness flap was elevated and the calvarium was exposed. Four circular defects with a diameter of 8 mm and a depth of 2 mm were created using a trephine bur without damaging the underlying dura mater and cerebral tissue under copious saline irrigation. The defects on the calvarium were randomly assigned to one of the four experimental groups. Each allocated defect was filled according to the study design. After material placement, the flaps were carefully closed and sutured using an absorbable 4-0 sutures (Monosyn, Braun, Terrassa, Spain). General antibiotic therapy using enrofloxacin (10 mg/day) was administered for 5 days after the operation.

6. Analysis

Clinical observations

Any possible inflammatory signs and unexpected complications of the surgical site were observed each day until the euthanizing at 2 and 8 weeks after surgery. No signs of infection, swelling, inflammation, or wound dehiscence were observed, and no rabbit in

this study was lost during the study period.

Micro-CT analysis

The calvarial defect specimens (2- and 8-week groups included 10 specimens each) were fixed with 10% formalin for 7 days and then scanned using micro-CT (SkyScan 1173, Bruker CT, Kontich, Belgium) at a pixel size of 13.93 μm (achieved using 130 kV and 60 μA). Scanned data sets were processed in the Digital Imaging and Communications in Medicine format, and reconstructed using 3D reconstruction software (Nrecon reconstruction program version 1.7.0.4, Bruker CT, Kontich, Belgium).

The region of interests (ROIs) for volume measurement in the CT analysis were defined as follows:

- Superior border: the mucoperiosteal layer covering the defect.
- Lateral border: the margins of the original defect.
- Inferior border: the dura mater.

Radiopaque areas were distinguished from the total augmented area using 8-bit threshold grayscale values at a pixel size of 13.93 μm . Grayscale values ranging from 50 to 255 were considered to indicate all mineralized tissue, with those from 50 to 90 considered to indicate newly mineralized tissue in the defects. Values higher than 90 and lower than 50 were considered to indicate BCP material and fibrovascular connective tissue, respectively. Within the ROIs, the following volumes were measured using the software.

- Total augmented volume (TAV; mm^3): total volume including fibrovascular connective tissue, newly formed bone, and grafted material volume within the ROIs.

- New bone volume (NBV; mm^3): sum of newly formed bone volumes in the defect.
- Residual material volume (RMV; mm^3): residual grafted material volume in the defect.

Histomorphometric analysis

After euthanizing the rabbits of each experimental group, tissue fixation was performed in a formalin solution at 4°C for 1 week. Micro-CT was performed before cutting each calvarial specimen. We prepared 20 tissue specimen slides by cutting the calvarial defect longitudinally. Hematoxylin-eosin was applied to un-decalcified and resin-embedded bone sections to distinguish the mineralized bone matrix from osteoid.

Histological slides were initially scanned using a digital slide scanner (Pannoramic 250 FLASH III, 3DHISTECH, Budapest, Hungary). After microscopic observations of the entire slides including various tissues, the slide images were digitally captured. A slide image analysis program (CaseViewer 2.1, 3DHISTECH) was used for histomorphometric analysis, and the data measured on scanned images were summarized in Excel.

The margins of the ROIs were defined by the defect cut made by the trephine bur. The superior and inferior borders of the ROI were defined by the periosteum and dura mater, respectively. Within the ROI, the following parameters were measured using the software:

- Total augmented area (TAA; mm^2): total area including fibrovascular connective tissue, newly formed bone, and grafted material volume in the ROI.
- New bone area (NBA; mm^2): sum of area of newly formed bone volume in the ROI.

- Residual material area (RMA; mm^2): residual grafted material area in the ROI.

Statistical analysis

SPSS software (IBM SPSS Statistics 26, SPSS, Chicago, IL) was used for the statistical analysis. TAV, NBV, and RMV measurements from micro-CT using grayscale and TAA, NBA, and RMA measurements from histomorphometrics and histology were summarized by mean \pm standard-deviation values. Kruskal-Wallis and Mann-Whitney U tests were used to analyze the statistic differences among the study groups at each time period (2 and 8 weeks) and between the same groups with different healing periods. Probability values of $p < 0.05$ were considered statistically significant.

III. RESULTS

1. Clinical observations

All experimental sites healed uneventfully and were maintained without complications such as infection or wound dehiscence during the study period. At sacrifice, all BCP blocks remained within the grafted site (Fig. 4C and D).

2. Micro-CT volumetric analysis

At 2 weeks, NBV was significantly larger in the BCP block 0.8-, 1.0-, and 1.2-mm groups (16.76 ± 3.36 , 15.06 ± 2.77 , and 16.02 ± 3.61 mm³, respectively) than in the control group (6.56 ± 3.53 mm³) ($p < 0.05$) (Table 1), and did not differ significantly between the BCP groups. TAV was also significantly larger in the BCP groups (161.86 ± 8.06 , 177.21 ± 26.96 , and 177.35 ± 18.40 mm³, respectively) than in the control group ($p < 0.05$), also with no significant difference between the BCP groups ($p > 0.05$). RMV was significantly larger in the 0.8-mm group (67.89 ± 5.75 mm³) than in the 1.0-mm (28.24 ± 3.65 mm³) and 1.2-mm (31.19 ± 1.24 mm³) groups ($p < 0.05$).

At 8 weeks, NBV was largest in the 1.0-mm group (35.81 ± 5.73 mm³), followed by the 1.2-mm (34.10 ± 5.91 mm³), 0.8-mm (32.02 ± 3.41 mm³), and control (24.11 ± 1.79 mm³) groups. All BCP groups had significantly larger NBVs than the control group, with no significant difference between the BCP groups. There were no significant differences in TAV between the BCP groups, which was larger in the 1.2- and 0.8-mm groups (190.33 ± 16.60 mm³ and 189.91 ± 24.60 mm³, respectively) than in the control group (151.68 ± 16.94 mm³). RMV was significantly larger in the 0.8-mm group (70.53 ± 5.52 mm³) than in the 1.0-mm (33.78 ± 2.68 mm³) and 1.2-mm (34.69 ± 3.09 mm³) groups

When 2- and 8-week groups were compared, all animals in the 8-week group had significantly larger NBVs than the corresponding 2-week animals (Table 1, Fig. 5A and Fig. 6). TAVs did not differ significantly between the 2- and 8-week groups.

3. Histomorphometric analysis

At 2 weeks, NBA was significantly larger in the 0.8-, 1.0-, and 1.2-mm BCP groups (0.30 ± 0.17 , 0.38 ± 0.38 , and 0.39 ± 0.19 mm², respectively) than in the control group (0.09 ± 0.06 mm²) ($p<0.05$) (Table 2), and did not differ significant between the BCP groups. TAA was also significantly larger in all BCP groups (15.74 ± 1.95 , 15.88 ± 1.00 , and 16.83 ± 1.24 mm², respectively) than in the control group (6.13 ± 1.13 mm²) ($p=0.008$). The 0.8-mm group had the largest RMA (9.61 ± 2.14 mm²), but the difference was not statistically significant.

At 8 weeks, NBA was only significantly larger in the 1.0-mm group (3.42 ± 0.48 mm²) than in the control group (2.26 ± 0.59) ($p=0.032$). Among the BCP groups, NBA was significantly larger in the 1.0- and 1.2-mm groups than in the 0.8-mm group. TAA was significantly larger in the 0.8-, 1.0-, and 1.2-mm BCP groups (16.52 ± 0.84 , 15.85 ± 1.04 , and 15.88 ± 1.29 mm², respectively) than in the control group (5.78 ± 1.10 mm²) ($p<0.05$), with no significant difference between the BCP groups. RMA was significantly larger in the 0.8-mm group (11.57 ± 0.81 mm²) than in the 1.0-mm (5.24 ± 0.14 , $p=0.016$) and 1.2-mm (4.70 ± 0.59 , $p=0.008$) groups.

Comparison of the 2- and 8-week groups revealed that all animals in the 8-week group had significantly larger NBVs than the corresponding 2-week animals in (Table 2, Fig. 5B and Fig. 7). RMA was significantly larger at 8 weeks than at 2 weeks ($p<0.05$).

4. Histological observations

Control group

In the control group, at 2 weeks the defect was partially filled with connective tissue and the center of the defect was sunk down and had a reduced total volume. New bone formation started from the adjacent native bone at the defect periphery (Fig. 7).

At 8 weeks, none of the defects were fully filled with new bone, and some bony islands and bone bridges were observed (Fig. 7).

0.8-mm group

In the 0.8-mm group, at 2 weeks the volume and shape of the defect were maintained by the BCP block and was completely encapsulated by fibrovascular tissue. The formation of new blood vessels for bone regeneration was observed and the initial bone regeneration started at the calvarial defect periphery (Fig. 7).

At 8 weeks, the BCP blocks remained in place without notable degradation, and new bone formation was observed from the periphery to the center along the surface of the BCP block. However, the new bone had not merged together. New bone formation was also observed in the pore area and mature bone was observed from the periphery of the defect. Overall, remarkable bone regeneration and growth patterns were observed in the BCP block close to the dura mater (Fig. 7).

1.0-mm group

In the 1.0-mm group, at 2 weeks the BCP block maintained the morphology of the formed defect, and an initial healing pattern was observed. Most of the interspaces between the BCP block lattice structure were filled with fibrovascular tissue, but loosely structured tissue was observed in the center of the BCP block. A concave lower boundary due to brain tissue pressure was observed on the dura mater contacting the BCP block (Fig. 7).

At 8 weeks, the 1.0-mm group presented the most new bone formation among the groups using BCP blocks, and bone regeneration occurred on all BCP block surfaces. A ring-shaped bone regeneration pattern was observed surrounding the BCP block surface. The new bone was also fused and matured using a connecting lattice structure pattern in

the BCP block (Fig. 7).

1.2-mm group

At 8 weeks, various bone growth types were observed in the 1.2-mm group. Ring-shaped new bone regeneration was observed surrounding the BCP block near to the dura mater (Fig. 7). At the upper part of the BCP block, osteogenesis was observed in a semilunar rather than a ring shape. However, regenerated bone fusion was not observed, indicating an independent bone regeneration pattern including independent island-shape bone formation.

IV. DISCUSSION

3D-printing technology allows synthetic block bone substitutes to be produced in customized shapes for application in bone augmentation procedures(Sohn, Park et al. 2010, Hwang, Park et al. 2012, Pae, Kang et al. 2019, Pae, Kang et al. 2019). However, the optimal pore diameter within the blocks is yet to be established. The main outcomes of this study were as follows: i) new bone formation was greatest with a pore diameter of 1.0 mm, ii) TAV was maintained in all BCP groups up to 8 weeks, as were the volume of remaining materials, and iii) appositional new bone growth was observed histologically around the lattice structure of the BCP blocks, with almost full defect closure at 8 weeks.

The BCP block bone substitute used in this study had a lattice structure composed of parallel cylindrical rod layers constructed on top of each other in a perpendicular arrangement. Consistent with the results of previous studies, the pore diameter in this study refers to the uniform gap between the rods inside the lattice, and new bone was observed to regenerate in this space(Tarafder and Bose 2014, Rh Owen, Dard et al. 2018). A previous study suggested that the pore diameter of block bone substitutes (HA scaffolds with small [90–120 μm] and large [350 μm] diameters) for enhancing vascularization and new bone formation should be larger than 300 μm (Tsuruga, Takita et al. 1997, Kuboki, Jin et al. 2001, Karageorgiou and Kaplan 2005), since pores smaller than 300 μm induced hypoxic conditions that suppressed direct bone regeneration(Jin, Takita et al. 2000, Kuboki, Jin et al. 2001, Kuboki, Jin et al. 2002). Consistent with that study, greater bone regeneration was achieved with BCP block substitutes with a larger pore diameter of 500 μm in other studies(Gauthier, Bouler et al. 1998, Chang, Lee et al. 2000). In contrast, a previous study using pure β -TCP block substitutes in rabbit calvaria found that bone formation was greater for the smallest pore diameter of 100 μm than for diameters of 250 and 400 μm (Diao, OuYang et al. 2018). However, this result might be explained by the greater

biodegradability of β -TCP compared with HA. Considering the lower biodegradability of HA compared with β -TCP, a larger pore diameter with a higher ratio of HA in the mixture of biomaterials is needed (Sohn, Park et al. 2010, Pae, Kang et al. 2019, Pae, Kang et al. 2019). The present study used a HA-to- β -TCP at a ratio of 60:40, and the new bone formation was greatest for a pore diameter of 1.0 mm after 8 weeks of healing.

An ideal BCP block would maintain the space of the defect until the defect has been fully regenerated. The remaining material can be biodegraded and be replaced by new bone as long as there is sufficient new bone to facilitate dental implant placements (Hulbert, Young et al. 1970, Wang and Boyapati 2006). The optimal degradation rate may vary with the pore diameter, the bone defect configuration, and the individual healing ability of the patient (Hing 2004, Hing 2005). Nonetheless, the ultimate purpose of designing the best block structure with an adequate pore diameter is to accelerate the bone regeneration process. As indicated by the results of this study, BCP bone substitutes were unresorbed during the 8-week healing period regardless of the pore diameter, as indicated by the maintenance of TAV and the remaining material. Using this biomaterial, it therefore would be reasonable to assume that a larger pore diameter would allow greater bone formation. On the other hand, as the pore diameter increases, the lattice structure density decreases and the compression strength also consequently decreases (Tarafder, Dernel et al. 2015). The compression strengths, chemical stabilities, and cytotoxicities of BCP blocks with pore diameters of 0.8 to 1.4 mm have been previously reported, which accelerated bone regeneration without unwanted deformation or destruction of the BCP blocks. The BCP block used in the present study promoted bone regeneration without infection or unwanted complications, and exhibited excellent biocompatibility, biodegradability, osteoinductivity, and osteoconductivity. Predictable results can therefore be obtained by applying the customized BCP block using 3D printing to the challenging procedure of reconstructing a wide range of complex bone defects.

The histological analysis of this study revealed that new bone was regenerated along

the lattice structure in a BCP block with a pore diameter of 1.0 mm, and osseointegration fused the new bones, indicating accelerated bone regeneration. However, for the 1.2-mm pore diameter, bone regeneration occurred in a ring shape on the lattice structure surrounding the BCP surface, but the connection (fusion) between new bones did not appear and bone regeneration was independent. At the upper part of the BCP block, unlike the lower part adjacent to the dura mater, osteogenesis was observed in a semilunar rather than a ring shape. This might suggest that the dura mater contains greater osteogenic potential compared to the overlying connective tissues. These results differ from those of previous studies, in which larger pore diameters between the lattice structures induced better initial bone regeneration, and the critical pore diameter for the BCP block was thought to be between 0.8 and 1.2 mm. In this study, consistent with the findings of the previous studies, when the pore diameter became larger than the critical size, the fibrous tissue penetrated over the defect and bone regeneration was hindered. Further studies are therefore needed to investigate whether the use of a barrier membrane can prevent unwanted fibrotic tissue invasion at the surface of the block and improve the regenerative outcome.

In addition, synthetic BCP blocks are based on HA and β -TCP, which may enhance new bone regeneration rates in certain physiological conditions. As can be seen from the RMV/RMA results in this study that the volume was maintained during a sufficient healing period and new bone synthesis increased. Predictable results can also be obtained by increasing the suitability and initial stability in the challenging guided bone regeneration (GBR) procedure in the destroyed ridge defect by using the synthetic bone that can be customized using 3D printing. In addition, compared to the particle type, certain block graft types could reduce surgical times, and the risks of postoperative complications including infection, swelling, and morbidity.

In this study, a barrier membrane was not used, so that the effectiveness of the blocks per se could be compared with respect to various pore diameters. Nevertheless, since a

barrier membrane might provide cell-occlusion for the blocks with larger pore sizes, the regenerative outcome could be enhanced. Studies using block-type bone graft materials are still insufficient in the literature, and further studies should be performed using different combinations of barrier membranes and block bone grafts.

V. CONCLUSION

In conclusion, within the limitation of this study, BCP block substitutes with different pore diameter promoted faster bone regeneration than that in the natural healing group. Above all, the greatest new bone regeneration results were shown in 1.0mm pore diameter group at 8 weeks. In addition, the BCP blocks maintained volume and space for bone regeneration in a sufficient healing period and had greater osteoconductivity and biocompatibility without postoperative complications. Future studies should investigate more-challenging defect configurations prior to considering clinical applications.

REFERENCE

- Barone, A., et al. (2008). "Xenograft versus extraction alone for ridge preservation after tooth removal: a clinical and histomorphometric study." *J Periodontol* 79(8): 1370-1377.
- Chang, B. S., et al. (2000). "Osteoconduction at porous hydroxyapatite with various pore configurations." *Biomaterials* 21(12): 1291-1298.
- Chavda, S. and L. Levin (2018). "Human Studies of Vertical and Horizontal Alveolar Ridge Augmentation Comparing Different Types of Bone Graft Materials: A Systematic Review." *J Oral Implantol* 44(1): 74-84.
- Cheng, M. Q., et al. (2016). "A novel open-porous magnesium scaffold with controllable microstructures and properties for bone regeneration." *Sci Rep* 6: 24134.
- De Oliveira, J. F., et al. (2003). "Effect of process parameters on the characteristics of porous calcium phosphate ceramics for bone tissue scaffolds." *Artif Organs* 27(5): 406-411.
- Diao, J., et al. (2018). "3D-Plotted Beta-Tricalcium Phosphate Scaffolds with Smaller Pore Sizes Improve In Vivo Bone Regeneration and Biomechanical Properties in a Critical-Sized Calvarial Defect Rat Model." *Adv Healthc Mater* 7(17): e1800441.
- Gauthier, O., et al. (1998). "Macroporous biphasic calcium phosphate ceramics: influence of macropore diameter and macroporosity percentage on bone ingrowth." *Biomaterials* 19(1-3): 133-139.
- Hing, K. A. (2004). "Bone repair in the twenty-first century: biology, chemistry or engineering?" *Philos Trans A Math Phys Eng Sci* 362(1825): 2821-2850.
- Hing, K. A. (2005). "Bioceramic bone graft substitutes: influence of porosity and chemistry." *International journal of applied ceramic technology* 2(3): 184-199.
- Hulbert, S. F., et al. (1970). "Potential of ceramic materials as permanently implantable skeletal prostheses." *J Biomed Mater Res* 4(3): 433-456.
- Hwang, J. W., et al. (2012). "Comparative evaluation of three calcium phosphate synthetic block bone graft materials for bone regeneration in rabbit calvaria." *J Biomed Mater Res B Appl Biomater* 100(8): 2044-2052.
- Jin, Q. M., et al. (2000). "Effects of geometry of hydroxyapatite as a cell substratum in BMP-induced ectopic bone formation." *J Biomed Mater Res* 51(3): 491-499.

- Karageorgiou, V. and D. Kaplan (2005). "Porosity of 3D biomaterial scaffolds and osteogenesis." *Biomaterials* 26(27): 5474-5491.
- Kato, E., et al. (2014). "Biodegradation property of beta-tricalcium phosphate-collagen composite in accordance with bone formation: a comparative study with Bio-Oss Collagen® in a rat critical-size defect model." *Clin Implant Dent Relat Res* 16(2): 202-211.
- Kuboki, Y., et al. (2002). "Geometry of artificial ECM: sizes of pores controlling phenotype expression in BMP-induced osteogenesis and chondrogenesis." *Connect Tissue Res* 43(2-3): 529-534.
- Kuboki, Y., et al. (2001). "Geometry of carriers controlling phenotypic expression in BMP-induced osteogenesis and chondrogenesis." *J Bone Joint Surg Am* 83-A Suppl 1(Pt 2): S105-115.
- Lee, J.-S., et al. (2018). "Alveolar ridge regeneration of damaged extraction sockets using deproteinized porcine versus bovine bone minerals: A randomized clinical trial." *Clinical Implant Dentistry and Related Research* 20(5): 729-737.
- Lim, H. K., et al. (2020). "3D-Printed Ceramic Bone Scaffolds with Variable Pore Architectures." *Int J Mol Sci* 21(18).
- Lim, T. C., et al. (2010). "Cryogenic prototyping of chitosan scaffolds with controlled micro and macro architecture and their effect on in vivo neo-vascularization and cellular infiltration." *J Biomed Mater Res A* 94(4): 1303-1311.
- Pae, H. C., et al. (2019). "Bone regeneration using three-dimensional hexahedron channel structured BCP block in rabbit calvarial defects." *J Biomed Mater Res B Appl Biomater* 107(7): 2254-2262.
- Pae, H. C., et al. (2019). "3D-printed polycaprolactone scaffold mixed with β -tricalcium phosphate as a bone regenerative material in rabbit calvarial defects." *J Biomed Mater Res B Appl Biomater* 107(4): 1254-1263.
- Ramesh, N., et al. (2018). "Hydroxyapatite-polymer biocomposites for bone regeneration: A review of current trends." *J Biomed Mater Res B Appl Biomater* 106(5): 2046-2057.
- Rh Owen, G., et al. (2018). "Hydroxyapatite/beta-tricalcium phosphate biphasic ceramics as regenerative material for the repair of complex bone defects." *J Biomed Mater Res B Appl Biomater* 106(6): 2493-2512.
- Roccuzzo, M., et al. (2007). "Autogenous bone graft alone or associated with titanium mesh for vertical alveolar ridge augmentation: a controlled clinical trial." *Clin Oral*

Implants Res 18(3): 286-294.

- Roosa, S. M., et al. (2010). "The pore size of polycaprolactone scaffolds has limited influence on bone regeneration in an in vivo model." *J Biomed Mater Res A* 92(1): 359-368.
- Sohn, J. Y., et al. (2010). "Spontaneous healing capacity of rabbit cranial defects of various sizes." *J Periodontal Implant Sci* 40(4): 180-187.
- Tarafder, S. and S. Bose (2014). "Polycaprolactone-coated 3D printed tricalcium phosphate scaffolds for bone tissue engineering: in vitro alendronate release behavior and local delivery effect on in vivo osteogenesis." *ACS Appl Mater Interfaces* 6(13): 9955-9965.
- Tarafder, S., et al. (2015). "SrO- and MgO-doped microwave sintered 3D printed tricalcium phosphate scaffolds: mechanical properties and in vivo osteogenesis in a rabbit model." *J Biomed Mater Res B Appl Biomater* 103(3): 679-690.
- Tsuruga, E., et al. (1997). "Pore size of porous hydroxyapatite as the cell-substratum controls BMP-induced osteogenesis." *J Biochem* 121(2): 317-324.
- Wang, H. L. and L. Boyapati (2006). ""PASS" principles for predictable bone regeneration." *Implant Dent* 15(1): 8-17.

TABLES

Table 1. The results from micro-CT analysis.

Healing period	Group	TAV	NBV	RMV
2 weeks (n=5)	Control	132.28 [\pm 12.29]	6.56 [\pm 3.53]	-
	0.8 mm	161.86 [\pm 8.06] ^(a)	16.76 [\pm 3.36] ^(a)	67.89 [\pm 5.75]
	1.0 mm	177.21 [\pm 26.96] ^(a)	15.06 [\pm 2.77] ^(a)	28.24 [\pm 3.65] ^(b)
	1.2 mm	177.35 [\pm 18.40] ^(a)	16.02 [\pm 3.61] ^(a)	31.19 [\pm 1.24] ^(b)
8 weeks (n=5)	Control	151.68 [\pm 16.94]	24.11 [\pm 1.79] ^(c)	-
	0.8 mm	189.91 [\pm 24.60] ^(a)	32.02 [\pm 3.41] ^{(a),(c)}	70.53 [\pm 5.52]
	1.0 mm	170.93 [\pm 16.61]	35.81 [\pm 5.73] ^{(a),(c)}	33.78 [\pm 2.68] ^{(b),(c)}
	1.2 mm	190.33 [\pm 16.60] ^(a)	34.10 [\pm 5.92] ^{(a),(c)}	34.69 [\pm 3.09] ^{(b),(c)}

**Values are presented as mean [\pm standard deviation] (mm³)

TAV : Total augmented volume, NBV : New bone volume, RMV : Residual material volume

^{a)} Statistically significant difference compared to the control group.;

^{b)} Statistically significant difference compared to the 0.8mm group.

^{c)} Statistically significant difference compared to the corresponding 2-week group at 8-weeks.

Table 2. The results from histomorphometric analysis.

Healing period	Group	TAA	NBA	RMA
2weeks (n=5)	Control	6.13±1.13	0.09±0.06	-
	0.8 mm	15.74±1.95 ^(a)	0.30±0.17 ^(a)	9.62±2.13
	1.0 mm	15.88±1.00 ^(a)	0.38±0.38 ^(a)	5.15±1.19
	1.2 mm	16.83±1.24 ^(a)	0.39±0.19 ^(a)	5.51±0.59
8weeks (n=5)	Control	5.78±1.10	2.26±0.59 ^(c)	-
	0.8 mm	16.52±0.84 ^(a)	1.60±0.70 ^(c)	11.57±0.81
	1.0 mm	15.85±1.04 ^(a)	3.42±0.48 ^{(a),(b),(c)}	5.24±0.14 ^(b)
	1.2 mm	15.88±1.29 ^(a)	3.04±0.66 ^{(b),(c)}	4.70±0.59 ^(b)

Values are presented as mean [\pm standard deviation] mm².

TAA: Total augmented area, NBA: New bone area, RMA: Residual material area.

^{a)} Significantly greater than the control group.

^{b)} Significantly greater compared to the 0.8 group.

^{c)} Significantly greater compared to the corresponding 2-week group.

FIGURES

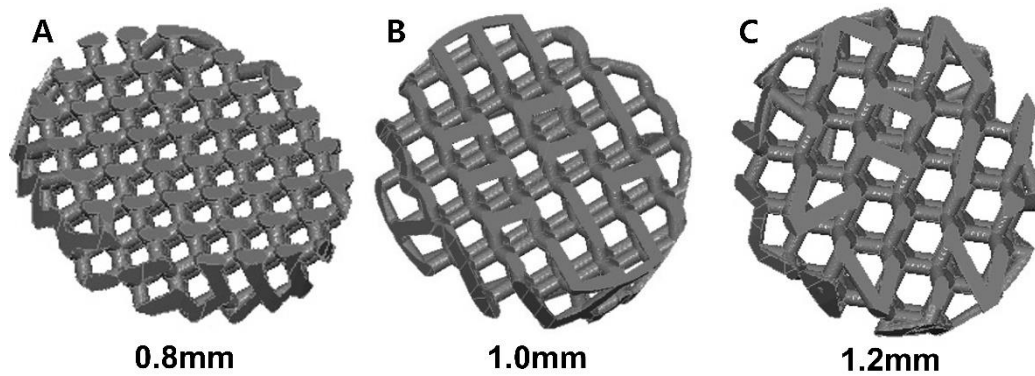


Figure 1. Structural design 3D- printed biphasic calcium phosphate(BCP) block bone substitutes.

A) BCP block with 0.8-mm pore diameter; B) BCP block with 1.0-mm pore diameter; C) BCP block with 1.2-mm pore diameter.

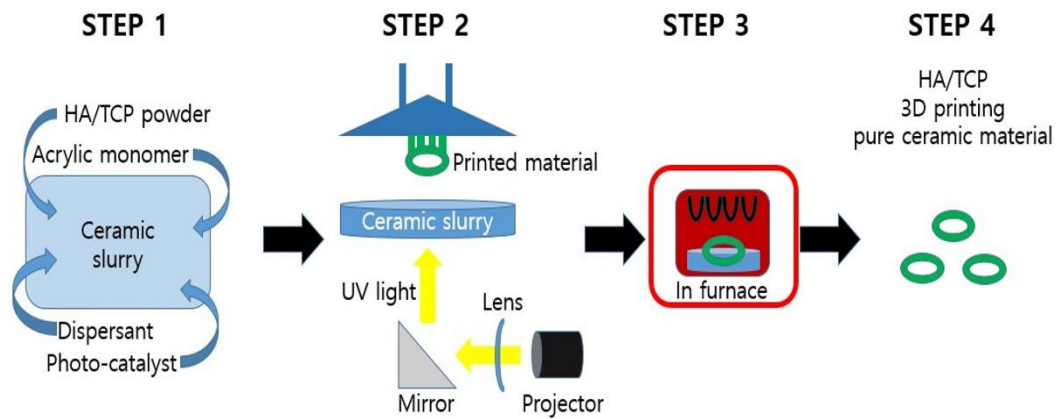


Figure 2. BCP block fabrication process by Digital Light Processing (DLP).

A) Photoreactive ceramic-resin composite composed of hydroxyapatite (HA)/ β -tricalcium phosphate (TCP), acrylic monomers, a dispersant, and a photo-catalyst were mixed in the ceramic slurry. B) Ultraviolet light was projected to polymerize the slurry and to form the specimen, which was attached to a build plate that slowly moved upward during printing. C) After the printing was completed, the polymer was completely removed using a heat-treatment step, where the scaffolds were sintered at 1250 °C for 10 h in an electrically heated chamber furnace in ambient air. D) The polymer residue was removed during sintering by pyrolysis, and the pure BCP block was obtained.

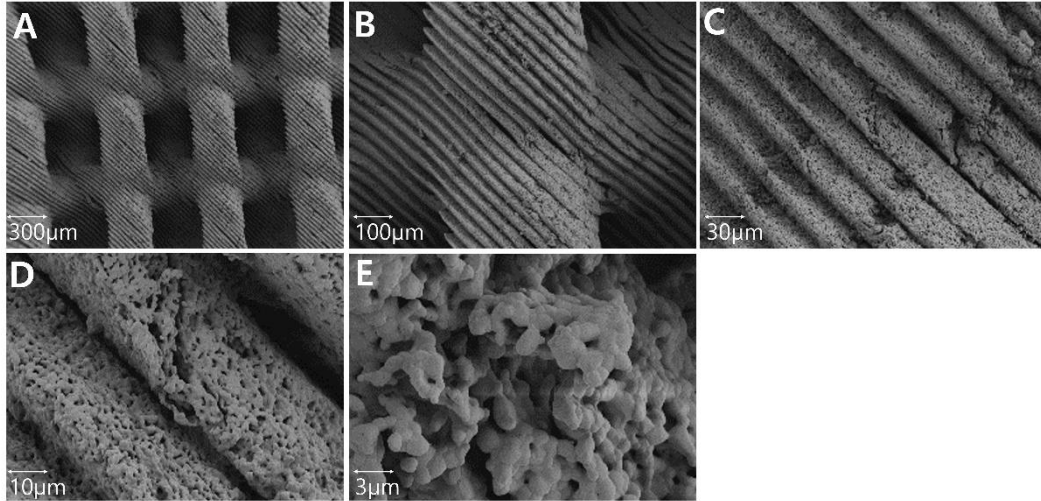


Figure 3. Microstructure surface images of 3D-printed BCP block using scanning electron microscopy (SEM, 3.0kV)

A) 30x; B)100x; C) 300x; D) 1,000x; E) 3,000x. All images showed pure BCP blocks without a residual polymer

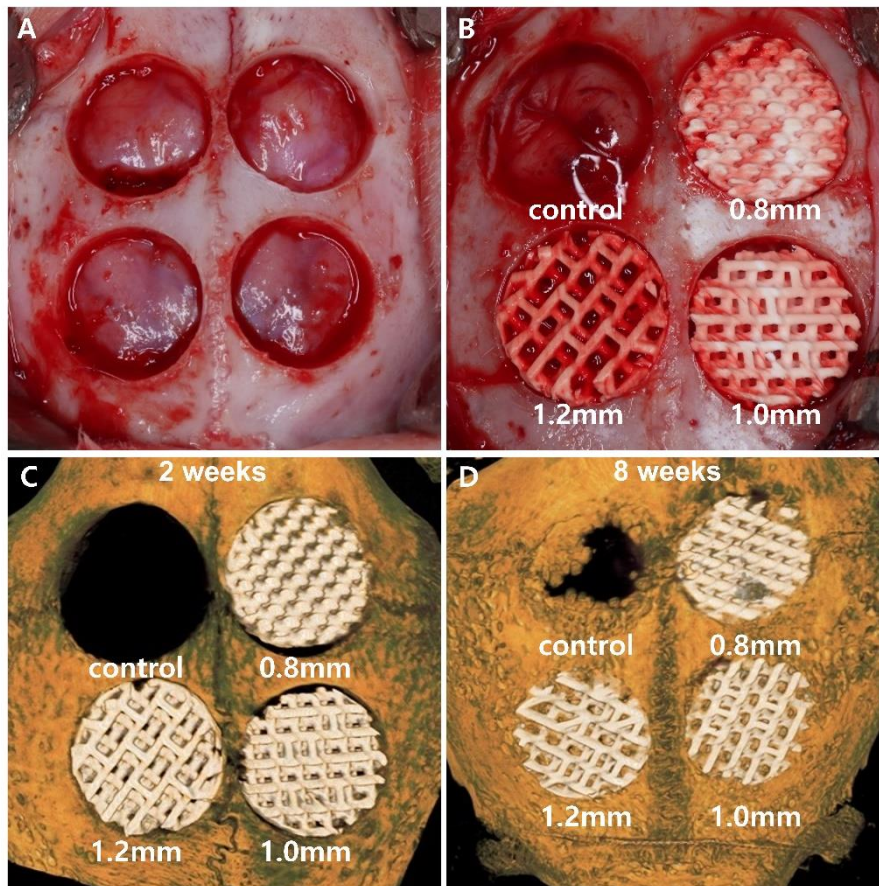


Figure 4. Study design and reconstructed images at 2- and 8- weeks.

A) 4 circular defects were prepared using a trephine bur 8 mm in diameter and 2 mm depth. **B)** Each defect was randomly allocated to one of four study groups. Clockwise from upper left: control group, empty; 0.8-mm group, BCP block with 0.8-mm pore diameter; 1.0-mm group, BCP block with 1.0-mm pore diameter; 1.2-mm group, BCP block with 1.2-mm pore diameter. **C)** Specimen at 2-weeks (Clockwise from upper left; control group, empty; 0.8-mm group; 1.0-mm group; 1.2-mm group) and **D)** specimen at 8-weeks (clockwise from upper left; control group, empty; 0.8-mm group; 1.0-mm group; 1.2-mm group).

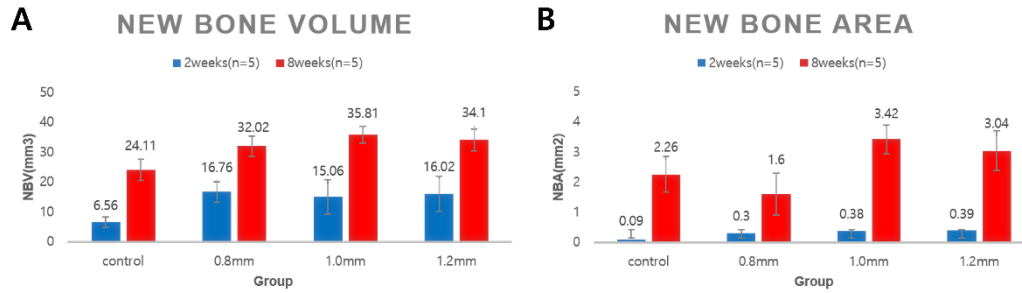


Figure 5. Comparison of A new bone volume (NBV) by micro-CT analysis and B new bone area (NBA) by histomorphometric analysis at 2- and 8-weeks.

**Values are presented as mean [\pm standard deviation].

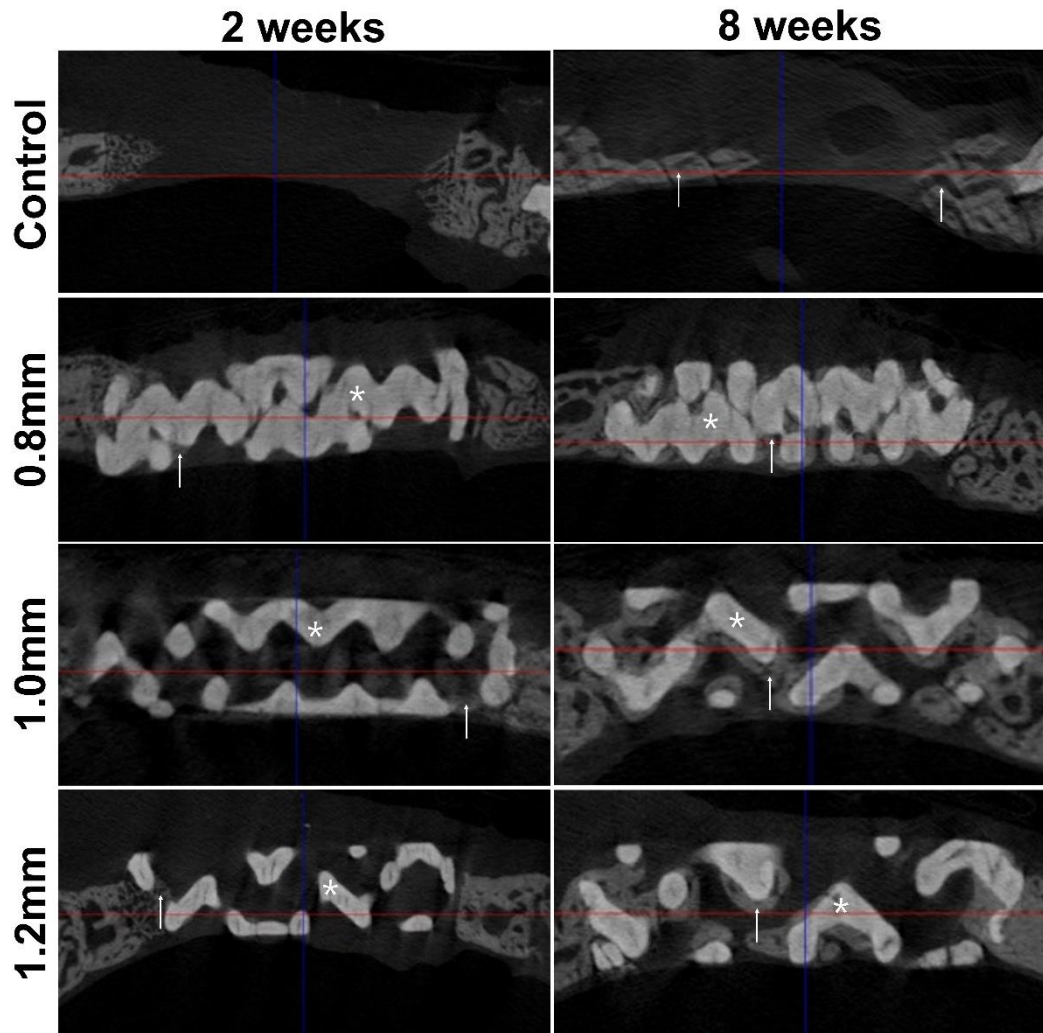


Figure 6. Micro-CT views at 2- and 8- weeks of healing period.

White asterisk: biphasic calcium phosphate (BCP) block. White arrow: regenerated new bone.

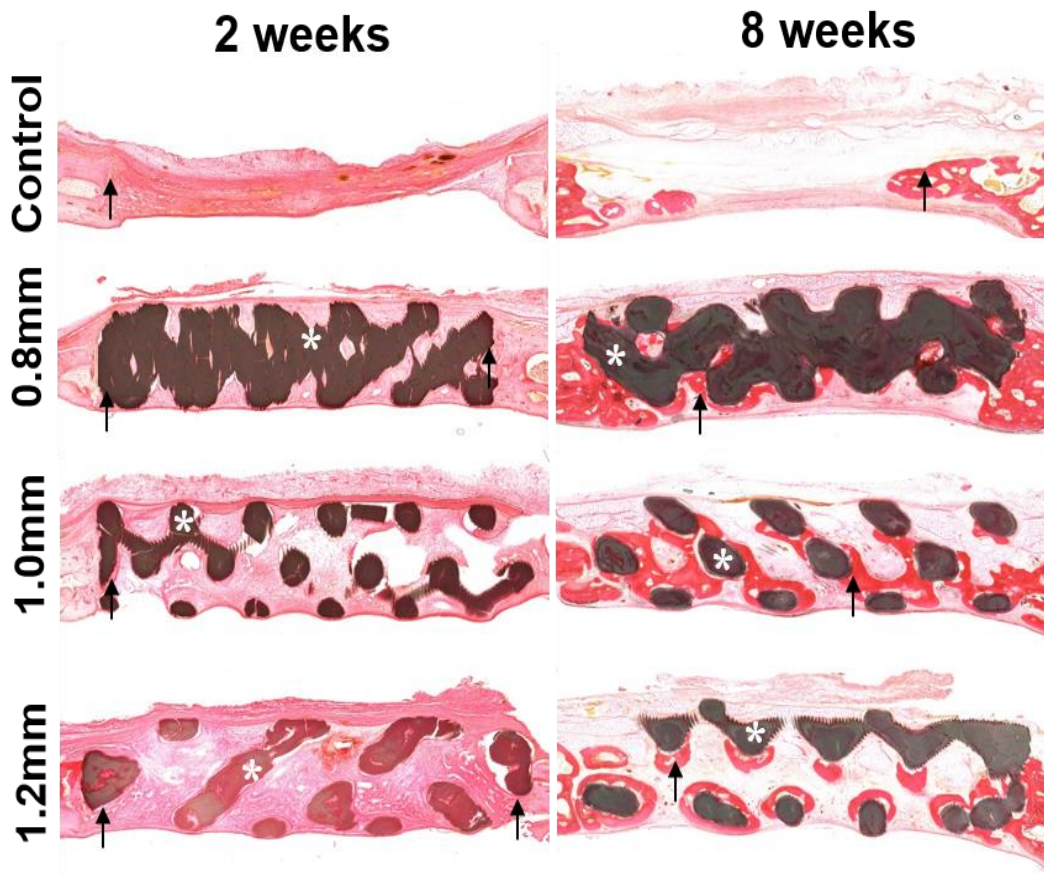


Figure 7. Histomorphometric views at 2- and 8-weeks of healing period.

White asterisk: biphasic calcium phosphate (BCP) block, black arrow: regenerated new bone.

국문요약

토끼 두개골에서 다른 기공 크기로 3차원적 프린트된 이상성 인산 칼슘 블록의 골재생 효과

<지도교수 최 성 호>

연세대학교 대학원 치의학과

서 영 욱

치조제증강술은 임플란트 식립을 용이하게 하기 위해 치조제결손부에서 흔히 시행된다. 노화 또는 치주 및 치근단 병리로 인해 치조제의 심한 흡수가 발생할 수 있다. 이러한 임상 상황에서 이식부위의 구조적 안정성을 위해 블록형태의 골이식재 사용이 제안되었다. 최근 3차원 프린트 기술의 발달으로 블록형 골이식재를 개인의 결손 형태에 맞게 맞춤화 할 수 있고, 생체 재료의 화학적 조성, 다공성 등의 특성을 조절할 수 있다.

이상성 인산 칼슘(Biphasic calcium phosphate)은 가장 흔히 사용되는 합성 골이식재료, 수산화인회석(hydroxy apatite)와 베타삼인산칼슘(beta tricalcium phosphate)의 조합으로 구성된다. 수산화인회석은 세포 이동, 혈관 형성 및 신생골 형성을 위한 골전도성 지지체를 제공하며, 인산칼슘은 자연골의 화학성분으로 우수한 생체적합성을 가지며 신생골 형성을 위한 칼슘 및 인산염 이온을 제공한다. BCP 블록에서 상호 연결된 기공의 존재는 세포의 침투 및 혈관 형성을 허용하며, 기공의 크기는 골형성 및 이식재의 흡수 속도에 영향을 줄 수 있다. 골 재생을 위한 최적의 기공 크기를 결정하기 위한 많은 연구가 있었지만, 그 결과는 아직 논란의 여지가 있다.

따라서 본 연구는, 토끼 두개골 결손 모델에서, 삼차원적으로 프린트된 서로 다른 기공 크기를 가지는 이상성 인산칼슘 블록의 골재생 효과를 임상적, 방사선학적 그리고 조직계측학적으로 비교 고찰하는 데에 목적을 두었다.

골재생 효과를 비교하기 위한 골 이식 재료로는 수산화인회석과 베타삼인산칼슘이 60:40 비율로 구성된 이상성 인산 칼슘(Biphasic calcium phosphate) 블록을 8mm (직경) x 2mm (높이)로 프린트하여 제작하였다. 10 마리의 토끼(male New Zealand white rabbit)를 대상으로 8mm (직경)의 트레핀 버(trephine bur)를 이용하여 두개골에서 4 개의 원형 결손부를 형성하고, 자연치유군(대조군), 0.8mm, 1.0mm, 1.2mm 기공 크기를 가지는 2 상성 인산 칼슘 블록군(실험군)으로 무작위로 적용하였다. 수술 후 2 주와 8 주에 각 5 마리의 실험동물을 희생한 후 채득한 시편을 염색하여 조직학적 관찰, 조직형태계측학적 분석을 시행하였고, 미세단층촬영(micro CT)을 시행하여 부피계측을 통해 두 군의 결과를 비교하였다. 동일 군내에서의 시간대별 통계적 비교를 위해서는 독립표본 t 검정을 시행하였고, 동일한 시기에서의 군간 통계적 비교를 위해서는 Kruskal-Wallis test, Mann-Whitney u test 를 시행하였다 ($p < 0.05$).

임상적으로, 전체 실험기간동안 감염, 창상 열개와 같은 합병증 없이 이상성 인산 칼슘 블록이 유지되며 치유됨을 확인하였다. 방사선학적 계측 결과, 이식재를 사용한 모든 2 주와 8 주 군에서 자연치유군에 비해 골재생이 유의하게 많은 결과를 확인하였고, 모든 8 주군은 2 주군에 비해 유의하게 많은 골재생이 관찰되었다. 조직형태계측학적 분석 결과, 2 주에서 모든 실험군은 자연치유군에 비해 유의하게 많은 골재생이 관찰되었고, 8 주에서 0.8mm 기공에 비해 1.0, 1.2mm 기공 그룹에서 유의하게 많은 골재생이 관찰되었다. 8 주군의 모든 실험군은 2 주군에 비해 유의하게 많은 골재생이

관찰되었다. 조직학적 관찰에서, 대조군은 결손부의 중심부위가 침하된 형태로 가장자리부터 신생골 재생이 관찰되었고, 0.8mm 군에서는 두개골 경막 가까이 위치한 골이식재의 표면을 따라 골재생이 일어남을 관찰하였다. 1.0mm 군에서는 모든 실험군 중 가장 뚜렷한 골재생과 함께 이식재를 둘러싼 신생골의 재생과 융합된 양상이 관찰되었다. 1.2mm 군에서는 이식재를 완전히 둘러싼 형태와 반만 둘러싼 형태의 골재생이 관찰되었으며, 신생골간의 융합은 관찰되지 않았다.

결론적으로, 서로 다른 기공 크기를 가지는 이상성 인산 칼슘 블록형 골이식재의 적용은 자연 치유그룹에 비해 골재생을 더 빠르게 촉진하였다. 특히, 8 주에서 1.0mm 의 기공크기에서 가장 많은 신생골 재생 결과를 보여주었다. 또한, 이상성 인산 칼슘 블록은 충분한 치유기간동안 술후 합병증 없이 이식부위의 공간과 부피를 유지하고 더 나은 골전도성과 생체적합성을 보여주었다. 후속 연구에서 임상적 적용 이전에 더 복합적인 결손 형태에 대한 적용과 골재생 효과에 대한 연구가 필요할 것이다.

핵심되는 말: 토끼 두개골 골이식, 골 재생, 기공 크기, 수산화인회석, 베타삼인산칼슘